JOURNAL OF AIRCRAFT
Vol. 34, No. 1, January–February 1997

Boundary-Layer Transition Detection in a Cryogenic Wind Tunnel Using Luminescent Paint

Keisuke Asai,* Hiroshi Kanda,† and Tetsuya Kunimasu†
National Aerospace Laboratory, Tokyo 182, Japan
and
Tianshu Liu‡ and John P. Sullivan§
Purdue University, West Lafayette, Indiana 47906

A technique for boundary-layer transition detection in a cryogenic wind tunnel has been developed. This technique is based on the thermal quenching of luminescent molecules. Calibration results show that luminescence of the paint composed of ruthenium complex and silicone polymer is strongly sensitive to temperatures over the range of 90–220 K. This capability allows one to visualize thermal signatures across the boundary-layer transition. A thin paint coating has been applied on three airfoil models with different thermal insulation properties. The paint was excited by a xenon light and the luminescence image was acquired using a high-resolution digital camera. To enhance the surface temperature signatures between laminar and turbulent regions, either the flow or the model substrate was cooled or heated in an active manner. Transition patterns have been successfully visualized by processing the luminescent images. Boundary-layer transition has been detected by using this technique over a cryogenic temperature range of 90–150 K in subsonic and transonic flows.

Nomenclature

c = chord length, m
cf = local skin friction coefficient
I = intensity, counts
k = thermal conductivity, W/K-m
l = thickness of an insulating layer, μm
p = pressure, kPa
q = heat flux, W/m^2
r = recovery factor
T = temperature, K
x = chordwise location, m
α = angle of attack, deg

Subscripts
aw = adiabatic wall
c = based on chord length
gas = working gas
heat = heating condition
in = insulating layer
lam = laminar
m = model
ref = reference
t = stagnation
tran = transient
turb = turbulent
w = wall

Presented as Paper 96-2185 at the AIAA 19th Advanced Measurement and Ground Testing Technology Conference, New Orleans, LA, June 17–20, 1996; received July 28, 1996; revision received Oct. 30, 1996; accepted for publication Nov. 5, 1996.

*Senior Researcher, Aircraft Aerodynamics Division. Associate Fellow AIAA.
†Research Engineer, Aircraft Aerodynamics Division.
‡Research Assistant, School of Aeronautics and Astronautics. Member AIAA.
§Professor, School of Aeronautics and Astronautics. Member AIAA.

Introduction

ONE of the major advances made in modern transonic wind-tunnel testing is the cryogenic wind-tunnel technology developed at NASA Langley Research Center.[1] A cryogenic wind tunnel provides a realistic means of simulating high Reynolds number flow. Cooling the test gas to near the liquid nitrogen (LN_2) temperature increases Reynolds number by more than a factor of 7. A large-scale pressurized cryogenic wind tunnel such as the National Transonic Facility (NTF) and the European Transonic Wind Tunnel (ETW) can achieve full-scale flight Reynolds number at transonic speeds with subscale models.

In these cryogenic wind tunnels, tests of aerodynamic models are usually performed with unfixed transition. Hence, the ability to detect the boundary-layer transition from laminar to turbulent flows is the most critical testing requirement for accurate drag estimation. To date, two types of transition detection techniques are available in a cryogenic wind tunnel. One is a multielement hot-film system[2–4] and the other is an infrared (IR) camera system.[5,6]

The multielement hot-film system can detect transition by measuring signals from an array of hot-film sensors that are vacuum deposited directly on the model surface. Johnson et al.[3,4] have demonstrated the capability of this technique for transition detection on airfoils near cryogenic conditions. A major disadvantage of this method is a lack of field mapping capability, which makes it unsuitable for measurement on complicated three-dimensional models.

In contrast, an IR camera system can provide a global picture of boundary-layer transition on a wing surface. This method is based on sensing small recovery temperature differences across transition lines. Gartenberg et al.[5] applied this technique to cryogenic wind-tunnel tests and succeeded in detecting boundary-layer transition on an airfoil model with fiberglass skin at temperatures down to 170 K. They used a standard IR camera that operates in the 8–12 μm wavelength. However, this type of IR camera cannot be used at lower cryogenic temperatures because the overall level of IR radiation rapidly decreases with decreasing temperature and the peak of the radiated energy is shifted to longer wavelengths. A special

long-wave IR camera having 0.3 K resolution at 100 K is needed and is currently being developed in ETW.[7]

In this paper, we present a new technique for global transition detection in a cryogenic wind tunnel. This technique is based on the thermal quenching of luminescent materials. Since the late 1980s, temperature-sensitive paint (TSP) and pressure-sensitive paint (PSP) have attracted much attention in the aerospace community. Using the luminescent paints, surface temperature and pressure distributions on aerodynamic models can be obtained using a standard imaging camera and digital image processing techniques. The principles of the TSP and PSP techniques are described in detail in the review papers by McLachlan and Bell[8] and Liu et al.[9]

Recently, various temperature-sensitive paints for aerodynamic applications have been developed.[10–13] A number of excellent TSPs in different temperature ranges have been discovered,[12,13] including several paints working at cryogenic temperatures. Like IR imaging, the TSP technique can visualize thermal signatures over a whole model surface such that transition location can be detected. This technique has been successfully applied to transition detection tests in conventional ambient-temperature wind tunnels.[11,12,14]

The objective of this study is to demonstrate the feasibility of the TSP technique for boundary-layer transition detection in a cryogenic wind tunnel. A thin paint coating composed of ruthenium complex and silicone polymer was applied on three airfoil models with different insulation properties. The tests were conducted for subsonic and transonic speeds in the 0.1-m Transonic Cryogenic Wind Tunnel (0.1-m TCWT) at the National Aerospace Laboratory (NAL). The stagnation temperature varied from 150 to 90 K. In this study, emphasis is placed on evaluating the paint system, the model materials, and insulating layers. Also, methods of enhancing temperature difference across the transition line are studied in detail. The experimental data are compared with the calculations by a simple thermal analysis in an attempt to establish the methodology for estimating the insulating-layer thickness necessary for boundary-layer transition detection.

Description of Experiment

Temperature-Sensitive Luminescent Paints

Temperature-sensitive paint for use in a cryogenic wind tunnel should have two characteristics: 1) high-temperature sensitivity over the operating range of a cryogenic wind tunnel and 2) robust attachment to the model surface at cryogenic temperature.

According to Campbell et al.,[13] two TSPs have high-temperature sensitivity at cryogenic temperature. They are 1) Ru(trpy) and 2) Ru(VH127) dissolved in a dimethylsiloxane polymer (Genesse Polymers Corp. GP197). Ru(trpy) and Ru(VH127) are ruthenium complexes synthesized in a laboratory and are not commercially available. Figure 1 shows luminescence intensity as a function of temperature for these paints. As shown, both Ru(trpy) and Ru(VH127) have a strong temperature dependence over the range of 90 to 220 K. The maximum logarithmic slope, $\Delta\, \ell n(I/I_{\text{ref}})/\Delta T$, is about -1.3 and -2.2% per degree for Ru(trpy) and Ru(VH127), respectively. Luminescence intensity decreases with increasing temperature. This results from the nonradiative deactivation that begins to dominate radiative transitions as the temperature increases. Interestingly, luminescence of these paints is very weak at ambient temperature.

Application of the paint on a model surface is another important concern. The paint must adhere to the surface strongly enough to withstand the flow. Also, the difference in thermal contraction between the paint and model must not create any cracks that may trigger premature transition. Since at cryogenic condition the boundary layer on the model is extremely thin because of the high unit Reynolds number and small-scale models, even very small cracks may trip the boundary layer.

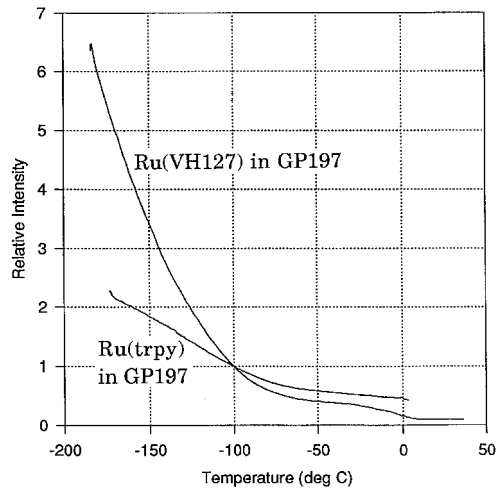

Fig. 1 Calibration curves for TSPs, Ru(trpy), and Ru(VH127) in GP197.

Tests of coating samples in a LN_2 Dewar indicate that the paint thickness is critical to prevent the coating from cracking or rippling. When the thickness is less than a certain critical value, the coating keeps smooth, even at cryogenic temperatures. This critical thickness is dependent on the model material and the paint itself.

Models and Insulating Layer

To enhance thermal signature induced by boundary-layer transition, aerodynamic models should be thermally insulated. In the present study, three airfoil models with different thermal insulation properties are used.

1) Model A: this model is made of machinable white glass ceramic, MACOR®.

2) Model B: this model is made of austenitic stainless steel (SUS304) covered with a white Mylar film, Monocoat®.

3) Model C: this model is also made of SUS304. Polyurethane (PU)-based white car paint is applied on the model surface for insulation.

To withstand high dynamic pressures, most models for cryogenic testing are made of stainless steel. However, the thermal conductivity of stainless steel is an order of magnitude higher than that of ceramic (16.3 vs 1.7 W/m-K at room temperature). Therefore, stainless models are required to be covered with adequate insulating layers, such as Mylar film and PU paint coating. To determine the proper thickness of the insulating layers, a simple thermal analysis has been performed. The details of the analysis are given in the Appendix. A thicker coating provides good thermal insulation, whereas a thinner coating is desirable for strong attachment. The suitable insulation thickness has to be determined by a tradeoff between these conflicting requirements.

The cross section of each model is identical and a symmetrical NACA 64A012 laminar airfoil. The chord length is 50 mm and the span is 100 mm. A small roughness element was placed at the leading edge of each model to generate a turbulent wedge. A thin film resistance heater was installed inside model B to heat the model substrate uniformly. A thermocouple was embedded in each model to monitor the model base temperature. The ruthenium-based temperature-sensitive paint was sprayed with an airbrush onto the model surface. It is noted that all models have white backing to enhance luminescence emission. After being dried for hours, the painted model surface was finished with an aluminum oxide lapping sheet. The rms surface roughness indicated by a stylus instrument is less than 1 μm.

Table 1 Test conditions

Case	M	P_t, kPa	T_t, K	$Re \times 10^{-6}$	α, deg
A	0.40	110	150	1.16	−2.0
B	0.40	110	150	1.16	−2.0 to +2.0
C	0.40	110	150–90	1.16–2.45	−2.0
D	0.40	110–180	140	1.28–2.09	−2.0
E	0.40	190	90	4.24	−2.0
F	0.75–0.81	110	120	2.57–2.69	0, +2.0

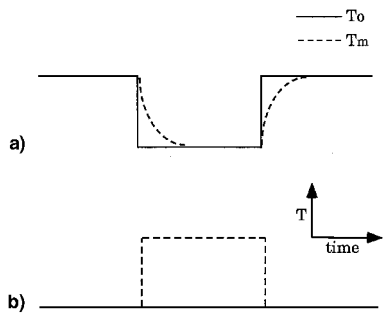

Fig. 2 Procedures of thermal signature enhancement techniques: a) transient and b) steady methods.

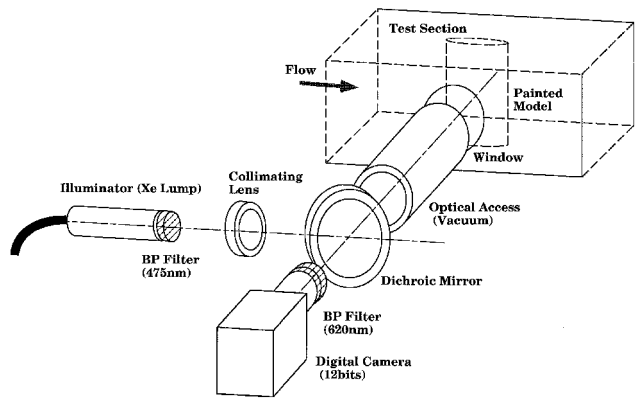

Fig. 3 Schematic of optical setup in the 0.1 m TCWT.

Thermal Signature Enhancement Technique

The adiabatic wall temperature difference ΔT_{aw} across transition line can be evaluated from the following simple relationship[14]:

$$\Delta T_{aw}/T_t = [M^2/(5 + M^2)]\Delta r \quad \text{where} \quad \Delta r = r_{turb} - r_{lam} \qquad (1)$$

The recovery factor values r are 0.84 and 0.896 for laminar and turbulent boundary layers, respectively. It is found from Eq. (1) that the temperature difference across transition line is very small at cryogenic freestream temperatures. For example, ΔT_{aw} is 0.17 deg for $M = 0.4$ and $T_t = 100$ K. In reality, it is difficult to resolve such a small temperature difference, even when using a 12-bit resolution camera, because of uneven paint thickness and lighting.

Since convective heat transfer coefficient in turbulent flow is much higher than in laminar flow, surface temperature difference between laminar and turbulent boundary-layer regions can be augmented by introducing an artificial increase of the temperature difference between the flow and the model. Two enhancement techniques have been employed in this study. One is called the transient method and the other is the steady method. Test procedures of these two methods are illustrated in Fig. 2. The transient method relies on heating or cooling of the tunnel stream (Fig. 2a). On the other hand, the steady method relies on heating the model substrate (Fig. 2b).

The transient method was used by Crowder[15] in an ambient transonic wind tunnel, and also by Gartenberg et al.[5] and Gartenberg and Wright[6] in a cryogenic wind tunnel. Note that the cryogenic wind tunnel is cooled by continuous LN_2 injection and a jump of the flow temperature can be easily induced by a rapid change in LN_2 flow rate. The steady method was employed by McLachlan et al.[14] for detecting transition in ambient wind-tunnel tests. An internal electric film heater is used to heat the model uniformly. The model temperature can be varied in a steady manner by controlling supply current.

In this experiment, we used a charge-coupled device (CCD) camera with the full well capacity of 60,000. Measurement accuracy is limited by photon shot noise and the maximum signal-to-noise ratio is approximated at 245. For Ru(trpy) paint, this corresponds to a minimum resolvable temperature difference of about 0.3°C. As discussed in the Appendix, the surface temperature jump across transition is about 30% of the difference between the model and flow temperatures (ΔT). This means that the ΔT threshold for transition detection is about 1 deg. Thus, ΔT was varied in this experiment from 1 to 5% of the freestream temperature for both the transient and steady methods.

Test Facility and Optical Setup

The transition experiments were conducted in the 0.1-m TCWT at NAL. This is a closed-circuit, fan-driven wind tunnel operated with cryogenic nitrogen as the working gas. Stagnation temperature can be varied from 90 to 200 K with the maximum stagnation pressure up to 200 kPa. The test section is 0.1-m square and equipped with slotted top and bottom walls of 4% porosity and solid sidewalls. The pressure fluctuation on the sidewall is about 1% and the mass-flux fluctuation in the test section is less than 0.3%.[16]

Figure 3 shows a schematic of an optical setup for this experiment. An excitation light source was a 300-W xenon lump with a light guide, a bandpass filter (475 ± 50 nm), and a collimating lens. A dichroic mirror was used to separate paint emission from excitation light. A digital camera with a cooled CCD (Hamamatsu, C4880) was used to detect the emission from the paint. This camera has a 12-bit gray-scale resolution and 1000 × 1018 pixel spatial resolution. A bandpass filter (620 ± 20 nm) was placed over the camera lens. A luminescent image was observed through a 70-mm-diam observation window on a sidewall of the test section. To avoid background noise because of the density fluctuations in a plenum chamber, an 88-mm-diam vacuum optical access was placed along the optical path.

Test Conditions

Test conditions in the 0.1-m TCWT are summarized in Table 1. Most tests were conducted at $M = 0.40$, $T_t = 150$ K, and $\alpha = -2$ deg (case A). Case B was performed to study the effect of angle of attack on boundary-layer transition. Cases C–E were carried out to study the effect of Reynolds number. Reynolds number ranges from 1.16 to 4.24 × 10^6, based on the chord length. Note that in a cryogenic wind tunnel, Reynolds number can be varied by changing either temperature or pressure. Case F was performed for studying the effect of Mach number.

Results and Discussion

Transition Images Obtained by the Transient Method

Figure 4 shows the response of the tunnel parameters to a step change in LN_2 injection. The Mach number is 0.4 and the stagnation temperature is 150 K at steady-state condition. The temperature jump is 7.5 K (5% of T_t). It is found that the cooling process is faster than the heating process. The time constant for cooling is less than 10 s. It is noted that a step change in T_t also disturbs the Mach number and the stagnation pressure. The maximum deviations of M and P_t from the steady-state values were 0.01 and 5 kPa. The luminescence intensity image was taken 2 s after introducing the temperature step. Thus, the disturbances in the freestream properties become much smaller when the transient image is taken.

Figure 5 shows the image processing sequence for the transient method. In this case, model B coated with Ru(trpy)-based paint was used. Figure 5a is a luminescent intensity image taken at the steady-state condition (M = 0.4 and T_t = 150 K, case A in Table 1), whereas Fig. 5b is taken during the cooling process ($\Delta T_t = -7.5$ K). The transient image (Fig. 5b) is a bit brighter than the steady-state image (Fig. 5a), since the former was taken during the cooling process. Transition signatures are not evident in these raw images because of uneven coating thickness, nonuniform illumination, and density fluctuation in the plenum chamber.

Figure 5c is a processed image obtained by subtracting Fig. 5b from Fig. 5a and then normalizing it with the steady-state image. The natural transition line is clearly identified as an edge of the brightness. The turbulent wedge induced by the leading-edge roughness is clearly visible as well. The turbulent region appears bright because it is cooled faster as a result of higher heat transfer. Obviously, the ratioing process has eliminated the effects of an uneven paint layer and nonuniform excitation. The intensity difference across the transition line is around 1.2% of I_{ref}, which corresponds approximately to a surface temperature difference of 1.5 K.

Figures 6a–6c show the images obtained with different temperature step increments ($\Delta T_t = -1.5$, -4.5, and -7.5 K), whereas Fig. 6d shows the image obtained during the heating process ($\Delta T_t = +7.5$ K). In the cooling cases (Figs. 6a–6c), the turbulent region is shown as a bright area, whereas in the heating case (Fig. 6d) the turbulent region is represented by a dark area. The transition image becomes much clearer with increasing temperature jump. One of the reasons for this contrast is that the spatial temperature gradient across the transition line increases with increasing step input.

It is known that the boundary-layer transition is sensitive to the nonadiabatic wall effects.[5,6] However, the natural transition location appears unchanged in Figs. 6a–6d. The airfoil model we used in this experiment has a favorable pressure gradient over a large portion of the surface, which makes the laminar boundary layer very robust until adverse pressure gradient prevails near the trailing edge. Therefore, the nonadiabatic wall effects are not significant for this particular model and at the present test condition.

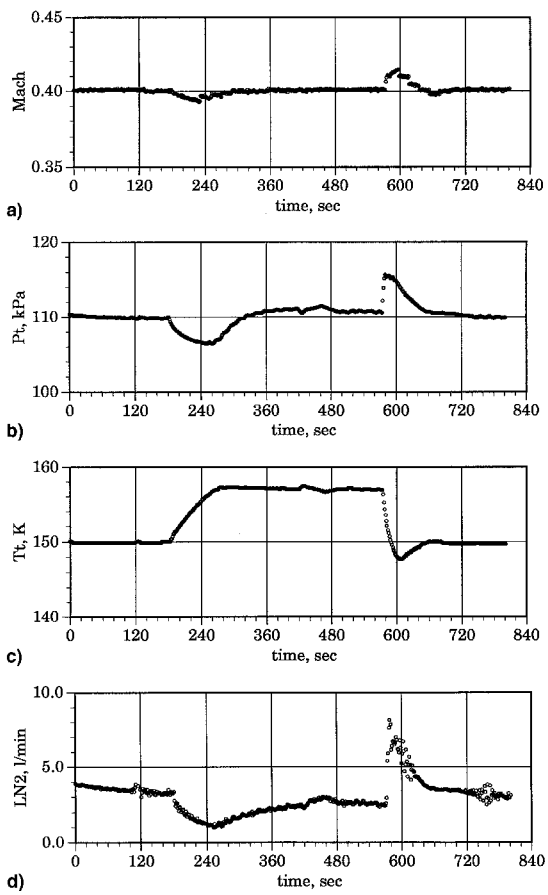

Fig. 4 Responses of the tunnel flow to a step change in LN_2 injection, M = 0.4, T_t = 150 K, and P_t = 110 kPa (baseline condition).

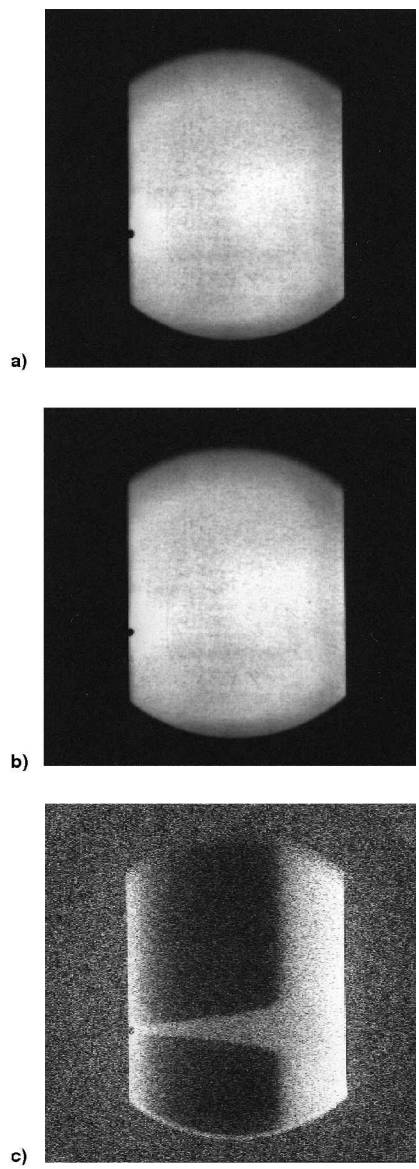

Fig. 5 Image processing sequence for the transient method, M = 0.4, T_t = 150 K, $\Delta T_t = -7.5$ K, model B, and Ru(trpy) paint: a) I_{ref}, b) I_{tran}, and c) $(I_{tran} - I_{ref})/I_{ref}$.

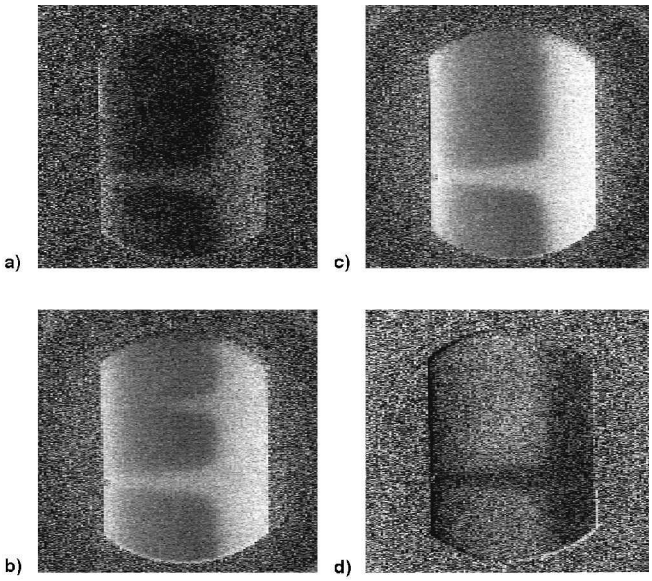

Fig. 6 Transition images for different step increments, $\Delta T_t/T_t$: a) −1, b) −3, c) −5, and d) +5%.

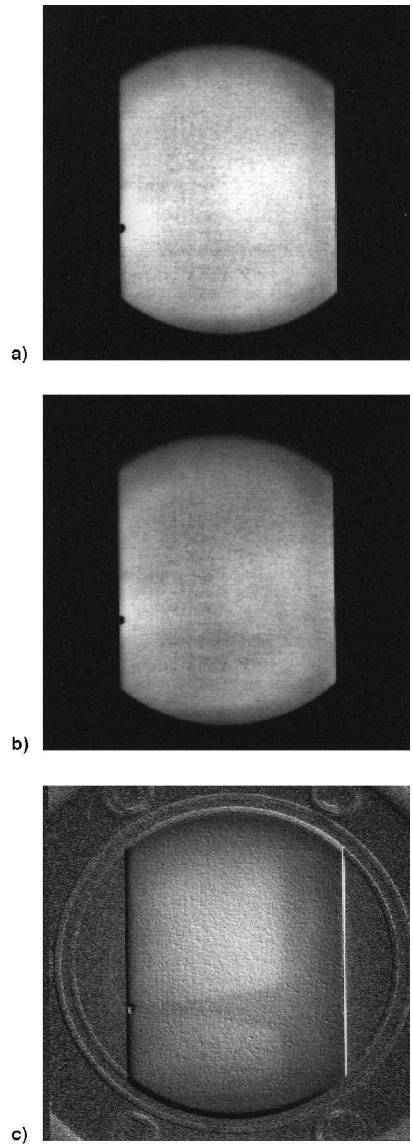

Fig. 7 Image processing sequence for the steady method, M = 0.4, T_t = 150 K, ΔT_m = +7.5 K, model B, and Ru(trpy) paint: a) I_{ref}, b) I_{heat}, and c) $(I_{ref} - I_{heat})/I_{ref}$.

Transition Images Obtained by the Steady Method

Boundary-layer transition can be visualized by using the steady method as well. Figure 7 shows the image processing sequence employed for the steady method. The test conditions are the same as in the transient method case shown in Fig. 5. Figure 7a is taken before the model is heated, whereas Fig. 7b is taken when the model is heated by $\Delta T_m (= T_m - T_t) = 7.5$ K. Contrary to the transient method, Fig. 7b is a bit darker than Fig. 7a, because the former shows the heated model surface.

Figure 7c is a processed image obtained by subtracting Fig. 7a from Fig. 7b, and then by normalizing it with Fig. 7a (the unheated image). Like the transient method, the steady method is able to visualize the natural transition line and the turbulent wedge as an evident edge of the brightness. It is noted that the edges of a rectangular film heater housed inside the model is barely visible in these images. For comparison, Figs. 8a–8c show the images obtained for a different heating rate (ΔT_m = 1.5, 4.5, and 7.5 K). It is observed that the contrast gets higher with increasing ΔT_m. Again, the nonadiabatic wall effects are negligible on the boundary-layer transition.

Comparison of Different Models

Figures 9a–9c compare the images for model A (MACOR), model B (stainless with Mylar film), and model C (stainless with PU paint coating). These images were taken at the same test condition (case A in Table 1, transient method, $\Delta T_t = -7.5$ K). Transition is clearly shown in all images. Among all of the models, model B provides the clearest transition image. Images for models A and C have about the same quality. This indicates that model B has the most suitable thermal insulating properties. Notice that the Mylar film applied on model B is relatively thick (50 μm), and an order of magnitude less heat conductive than MACOR.

Luminescence Profile Along Chordwise Direction

Figure 10 shows chordwise luminescence intensity profiles extracted from Fig. 5c at two spanwise locations. One is through a natural transition region and the other is through a forced transition region. Data of 10 spanwise and five chordwise pixels were averaged to reduce spatial noise. The plot clearly illustrates the evolution of the boundary layer from laminar to turbulent flows. The high-intensity region near the leading edge is caused by high local heat transfer in thin laminar boundary layer. The intensity decreases as the laminar boundary layer thickens and the local heat transfer decreases. The intensity jump at about x/c = 66% signifies the position of transition onset. Transition to turbulence is completed at about x/c = 79%.

Figure 11 shows chordwise luminescent profiles for three angles of attack (case B in Table 1, $\alpha = -2$, 0, and +2 deg). In these tests, model B coated with Ru(VH127) paint was used. As the angle of attack increases, the position of transition onset moves toward the leading edge. The transition location detected by the paint data is consistent with the theoretical prediction.

Effects of Reynolds Number on Transition Images

Figures 12 and 13 show the transition images taken at various Reynolds numbers. In these tests, model A coated with Ru(VH127) paint and the transient method ($\Delta T = 0.05 T_t$) were used. Figures 12a–12d represent images at various stagnation temperatures from 140 to 100 K (case C in Table 1), when the

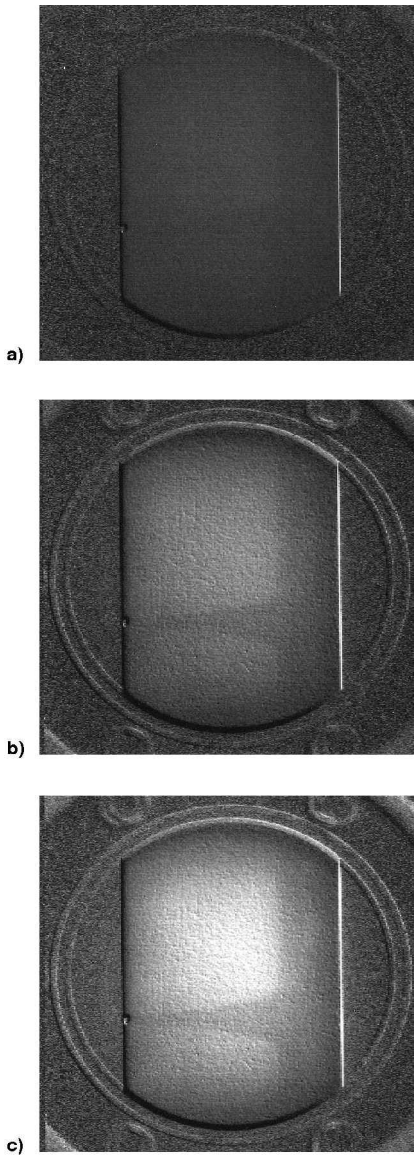

Fig. 8 Comparison of the images obtained for different heating rate. ΔT_m = a) 1.5, b) 4.5, and c) 7.5 K.

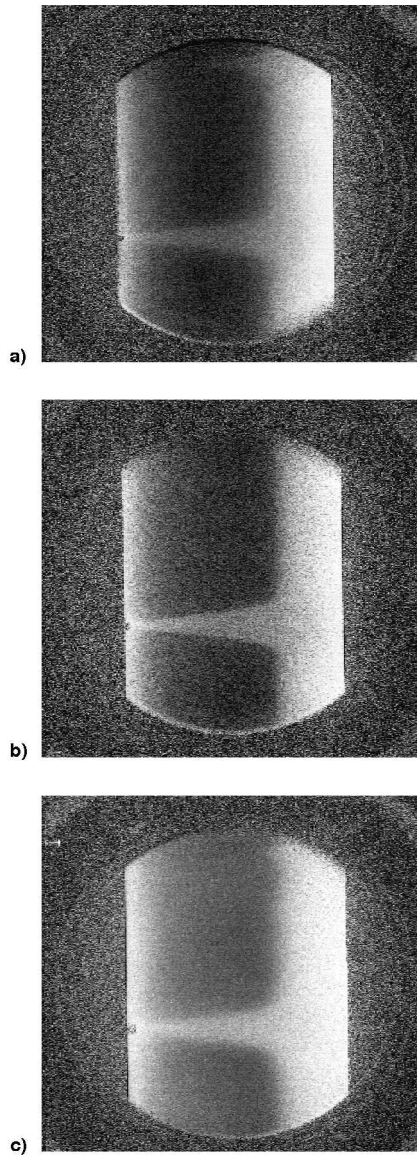

Fig. 9 Comparison of the images obtained with models having different thermal insulation properties: a) MACOR, b) SUS304+ Mylar film, and c) SUS304+PU paint.

tunnel stagnation pressure is constant (110 kPa). On the other hand, Figs. 13a and 13b show the images taken at a constant temperature (140 K) and at stagnation pressures of 156 and 180 kPa (case D in Table 1). It is noted that the Reynolds number in Figs. 13a and 13b are the same as those in Figs. 12c and 12d.

As shown in these figures, the number of turbulent wedges increases with increasing Reynolds number, whereas the location of a natural transition line appears unchanged with Reynolds number. The similar change in transition pattern can be observed through either way of adjusting Reynolds number. The turbulent wedges at higher Reynolds numbers are possibly caused by small imperfections near the leading edge having a size close to the critical roughness height. This interpretation is supported by an observation that the wedges disappear when the Reynolds number is decreased by rewarming the tunnel.

Figure 14 is the transition image taken at 90 K and 190 kPa. Reynolds number based on the chord length is 4.24×10^6, the highest value achievable in this tunnel. It is seen that most of the boundary layers are prematurely tripped at the leading edge. This image was obtained with model B and using the steady method, because transient cooling would cause liquefaction of the working gas. Some defects near the leading edge may be attributed to contamination of the paint layer, since new turbulent wedges appear as the run continues. The leading edge of the model was inspected through an optical magnifier after each run, but the defects of the paint layer were too small to observe with this method.

Images Obtained at Transonic Mach Numbers

Figure 15 shows a series of transition images taken near the critical Mach numbers and at $\alpha = +2$ deg (case F of Table 1). The steady method ($\Delta T_m = 10$ K) was used to avoid producing undesirable disturbances in freestream. An interesting feature shown in these images is that, besides the transition lines and the turbulent wedges, a shock wave spanning the model is clearly observed in the same image. It is seen that a weak shock forms at $M = 0.78$ and becomes stronger as the Mach number increases.

Notice that in Fig. 15 a shock wave appears as the dark and bright line. This is a well-known image of a shock wave in a shadowgraph. Remember that we used a near-parallel beam of

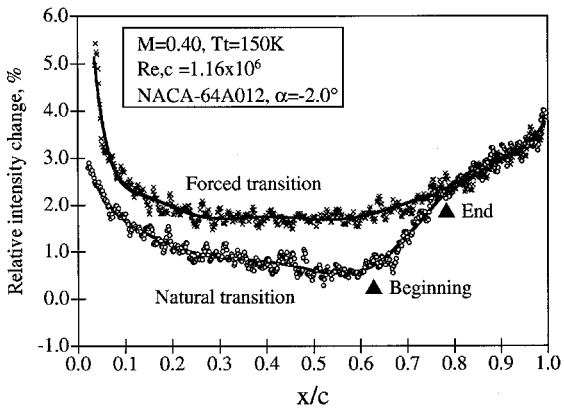

Fig. 10 Chordwise luminescent intensity profiles through forced and natural transition regions.

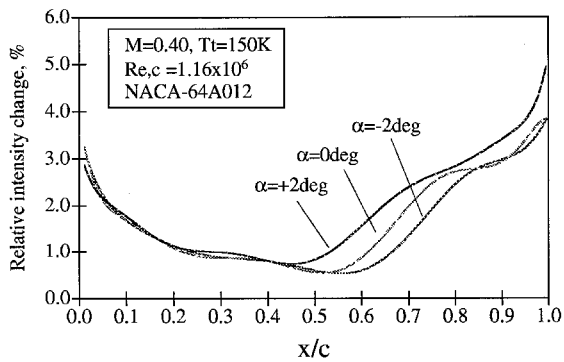

Fig. 11 Transition location variation from $\alpha = -2$ to $+2$ deg (case B).

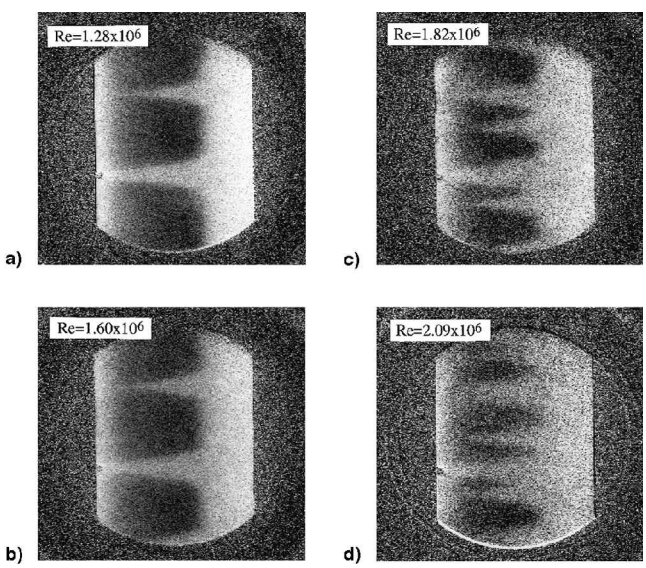

Fig. 12 Transition images obtained for varying Reynolds numbers (case C). T_t = a) 140, b) 120, c) 110, and d) 100 K; P_t is maintained at 110 kPa in all cases.

light to excite the luminescent paint. The model surface actually acted as an efficient screen for shadow projection. The shadow of a shock wave is relating to a change in the second derivative of the refractive index (or density) in a shock wave, thus appearing as the dark and bright contour. These figures illustrate the usefulness of the paint technique to capture the details of the flowfield, including boundary-layer transition and shock wave.

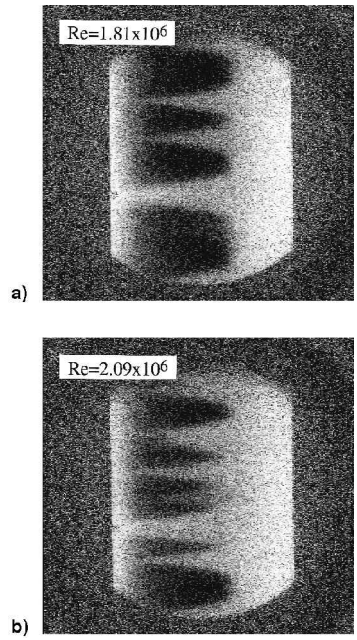

Fig. 13 Transition images obtained for varying Reynolds numbers (case D). P_t = a) 156 and b) 180 kPa; T_t is maintained at 140 K.

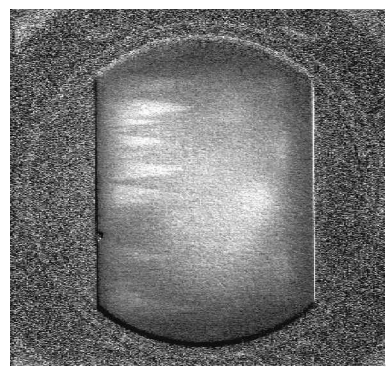

Fig. 14 Transition image taken at T_t = 90 K and P_t = 190 kPa (case D, $Re = 4.24 \times 10^6$).

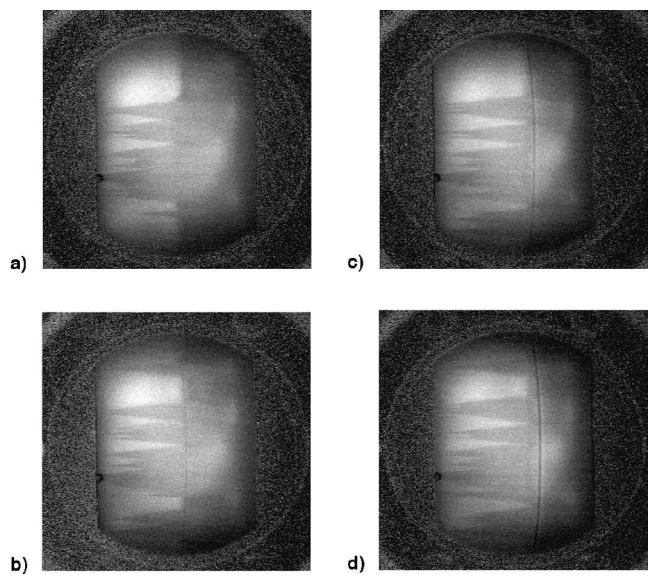

Fig. 15 Images obtained near the critical Mach numbers (case F). M = a) 0.76, b) 0.78, c) 0.80, and d) 0.81.

Conclusions

Based on use of the temperature-sensitive paint working at cryogenic temperature, a technique for global boundary-layer transition detection in a cryogenic wind tunnel has been developed. To demonstrate the feasibility of this technique, a series of systematic experiments has been conducted in the 0.1-m TCWT at NAL. The results obtained in this study are summarized as follows:

1) Using temperature-sensitive luminescent paint, boundary-layer transition on an airfoil model in a cryogenic wind tunnel has been successfully detected. This technique works at cryogenic temperatures down to 90 K.

2) Three airfoil models with different insulating properties have been compared. Transition can be visualized on all of these models. A paint-type insulation can survive at 90 K, which could be used on more complicated three-dimensional models.

3) The transient and steady methods have been successfully employed to augment spatial temperature signatures caused by transition. The steady method is useful, particularly at the minimum operating temperature and at transonic Mach numbers, where flow disturbances induced by a flow temperature jump are not allowed.

4) The calculations of surface temperature by the simple thermal analysis are in good agreement with the paint-derived data, except near the trailing edge. This simple method gives an easy way of estimating the insulating-layer thickness necessary for boundary-layer transition detection.

5) The effect of Reynolds number on boundary-layer transition have been studied using the paint technique. The change of transition patterns with increasing Reynolds number can be observed in the cases of both cooling and pressurizing the tunnel.

6) At transonic Mach numbers, a shock wave has been visualized as well in the transition image. An image of a shock wave is actually the shadow of a shock wave projected onto a luminescent model surface. Using a near-parallel beam of excitation light, it is possible to visualize the details of the complex flowfield, including boundary-layer transition and shock waves.

7) Even using a high-resolution camera, transition signatures are not observed in raw images. To obtain a transition image without using any enhancement techniques, further improvement in the paint system, optical-sensing technologies, and image-processing techniques is required.

Appendix: Thermal Analysis for Insulating-Layer Thickness Requirement

An analysis has been performed to determine the requirement for a thin insulating layer on metallic model. For simplicity, we consider steady-state one-dimensional heat transfer in thin insulating layer on a metallic model at constant temperature T_m.

From thermal balance at the insulating layer surface, the heat transfer rate q can be expressed by

$$q = Nu_x(k_g/x)(T_w - T_{aw}) = -(k_{in}/l)(T_w - T_m) \qquad \text{(A1)}$$

Assuming the Prandtl number is unity

$$T_{aw} = T_t \qquad \text{(A2)}$$

We also assume the following relation between skin friction and heat transfer (Reynolds analogy):

$$Nu_x = (c_f/2)Re_x \qquad \text{(A3)}$$

Combining Eqs. (A1–A3), we obtain

$$\frac{T_w(x) - T_t}{T_m - T_t} = \left(1 + \frac{c_f(x)}{2} Re_c \frac{k_{gas}}{k_{in}} \frac{l}{c}\right)^{-1} \qquad \text{(A4)}$$

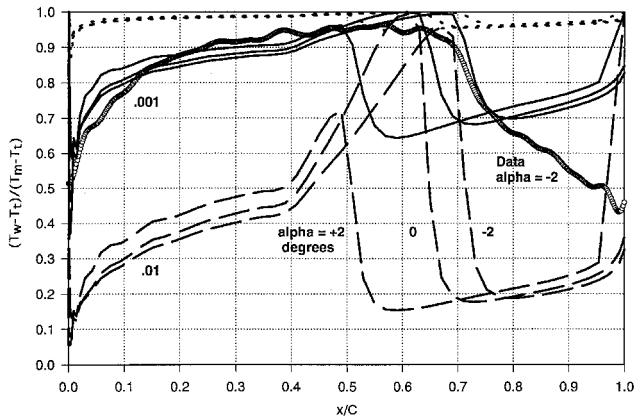

Fig. A1 Predicted surface temperature distributions for various insulation thicknesses, $M = 0.4$, $Re = 1.16 \times 10^6$, NACA 64A012, $\alpha = -2$ to $+2$ deg.

This formula gives the surface temperature distribution on a metallic model covered by a thin insulating layer with a given skin friction distribution and properties of an insulating layer.

Figure A1 shows surface temperature distributions for different insulating-layer thicknesses on the NACA 64A012 airfoil at different angles of attack for $M = 0.4$ and $Re = 1.16 \times 10^6$. The external flow and the boundary layers were calculated using the Euler and boundary-layer codes. The transition locations were estimated with the linear stability method (e^N method). The thermal conductivity of an insulating layer k_{in} is assumed to be 10 times as large as k_{gas}, representing a value for typical polymer insulation. The thickness l is varied from 10^{-4} to 10^{-2} of c. For $c = 50$ mm, the thickness ranges from 5 to 500 μm. As shown in Fig. A1, the T_w difference between laminar and turbulent regions increases with increasing insulating-layer thickness.

The data obtained by the paint technique at $\alpha = -2$ deg are also plotted in Fig. A1 for comparison. In this case, a stainless-steel model covered with a 50-μm-thick Mylar film (model B) was used. The experimental data are in good agreement with the simple analysis, except near the trailing edge. The steady-state thermal balance [Eq. (A1)] is no longer accurate near the very thin trailing edge. Hence, the calculation of the surface temperature deviates from the experimental data near the trailing edge. Nevertheless, this simple analysis gives an easy way of estimating the insulating-layer thickness necessary for boundary-layer transition detection.

Acknowledgments

We would like to thank Hideo Sawada, Takashi Kohno, and Yoshimi Iijima at NAL for their assistance in conducting tests in the 0.1-m TCWT. Also, we would like to acknowledge Brian Campbell at Purdue University for informative discussions on calibration results of the paints. Lastly, we are grateful to David R. McMillin and Corey Cunningham at the Department of Chemistry of Purdue University for providing Ru(trpy), and to Randolph P. Thummel of the University of Houston for providing Ru(VH127).

References

[1]Goodyer, M. J., and Kilgore, R. A., "The High Reynolds Number Cryogenic Wind Tunnel," *AIAA Journal*, Vol. 11, No. 5, 1973, pp. 613–619.

[2]Fancher, M. F., "A Transonic Wind Tunnel Test of a Supercritical Airfoil Model: Background and Progress," AIAA Paper 80-0418, March 1980.

[3]Johnson, C. B., Carraway, D. L., Stainback, P. C., and Fancher, M. F., "A Transition Detection Study Using a Cryogenic Hot Film System in the Langley 0.3-Meter Transonic Cryogenic Tunnel,"

AIAA Paper 87-0049, Jan. 1987.

[4]Johnson, C. B., Carraway, D. L., Hopson, P., Jr., and Tran, S. Q., "Status of a Specialized Boundary Layer Transition Detection System for Use in the U.S. National Transonic Facility," *International Congress on Instrumentation in Aerospace Simulation Facilities '87 Record*, June 1987, pp. 141–155.

[5]Gartenberg, E., Johnson, W. G., Jr., Johnson, C. B., Carraway, D. L., and Wright, R. E., "Transition Detection Studies in the Cryogenic Environment," AIAA Paper 90-3024, Aug. 1990.

[6]Gartenberg, E., and Wright, R. E., "Boundary-Layer Transition Detection with Infrared Imaging Emphasizing Cryogenic Applications," *AIAA Journal*, Vol. 32, No. 9, 1994, pp. 1875–1882.

[7]Anon., "Infrared Cameras for Transition Detection," *ETW News*, No. 1, May 1994.

[8]McLachlan, B. G., and Bell, J. H., "Pressure-Sensitive Paint in Aerodynamic Testing," *Experimental Thermal and Fluid Science*, Vol. 10, 1995, pp. 470–485.

[9]Liu, T., Campbell, B. T., Burns, S. P., and Sullivan, J. P., "Temperature- and Pressure-Sensitive Luminescent Paints in Aerodynamics," *Applied Mechanics Reviews* (to be published).

[10]Liu, T., Campbell, B. T., and Sullivan, J. P., "Thermal Paints for Shock/Boundary Layer Interaction in Inlet Flows," AIAA Paper 92-3626, July 1992.

[11]Campbell, B. T., Liu, T., and Sullivan, J. P., "Temperature Measurement Using Fluorescent Molecules," 6th International Symposium on Application of Laser Technique to Fluid Mechanics, Lisbon, Portugal, July 1992.

[12]Campbell, B. T., "Temperature Sensitive Fluorescent Paints for Aerodynamic Applications," M.S. Thesis, School of Aeronautics and Astronautics, Purdue Univ., West Lafayette, IN, May 1993.

[13]Campbell, B. T., Liu, T., and Sullivan, J. P., "Temperature Sensitive Fluorescent Paint Systems," AIAA Paper 94-2483, June 1994.

[14]McLachlan, B. G., Bell, J. H., Gallery, J., Gouterman, M., and Callis, J., "Boundary Layer Transition Detection by Luminescence Imaging," AIAA Paper 93-0177, Jan. 1993.

[15]Crowder, J. P., "Infrared Cameras for Detection of Boundary Layer Transition in Transonic and Subsonic Wind Tunnels," AIAA Paper 90-1450, June 1990.

[16]Sawada, H., and Aoki, T., "NAL 10-cm Cryogenic Wind Tunnel," *Proceedings of the 1st Pacific International Conference on Aerospace Science and Technology* (Tainan, Taiwan), 1993, pp. 1143–1150.